Reduced Occupancy of the Oxygen-Evolving Complex of Photosystem II Detected in Cryo-Electron Microscopy Maps

Jimin Wang,*,[†] Krystle Reiss,[‡] Gary W. Brudvig,[‡] and Victor S. Batista[‡]

[†]Department of Molecular Biophysics and Biochemistry, Yale University, New Haven, Connecticut 06520-8114, United States
[‡]Department of Chemistry, Yale University, New Haven, Connecticut 06520-8107, United States

S *Supporting Information*

ABSTRACT: Computational simulations of electrostatic potentials (ESPs), based on atomistic models and independent atomic scattering factors, have remained challenging when applied to the oxygen-evolving complex (OEC) of photosystem II (PSII). Here, we overcome that challenge by using an ESP function obtained with density functional theory and atomic coordinates for the OEC of PSII obtained by optimization of the dark-adapted S_1 state. We find that the ESP is much higher for the OEC than for the nearby reference side chain of amino acid residue D1-H190. In contrast, experimental ESP maps recently published for two PSII−light-harvesting complex II super-complexes show that the ESP of the OEC is approximately half the value of the D1-H190 side chain. The apparent disparity is attributed to a reduced 31−38% occupancy of the OEC, likely associated with its reduction by electron scattering.

Photosystem II (PSII) is responsible for water oxidation to generate molecular oxygen that supports all aerobic life on the planet. It has been a subject of extensive biochemical, biophysical, and theoretical studies using methods such as X-ray crystallography and quantum mechanics.[1−3] It was found that the oxygen-evolving complex (OEC) is reduced upon X-ray irradiation.[4] Most recently, cryo-electron microscopic (EM) structures reported for spinach PSII−light-harvesting complex II (LHCII) supercomplexes at ∼3.2 Å resolution (EMD 6617 and PDB 3JCU; EMD 6742 and PDF 5XNM) provide experimental electrostatic potential (ESP) functions and thus information about the ionic charges in the supercomplexes.[5,6] We are interested in information provided by these structures about the Mn_4CaO_5 cluster that catalyzes the water-oxidation reaction in the OEC of PSII, particularly information about whether the OEC is also reduced upon electron irradiation.

Fourier transformation of the molecular ESP function results in the electron structure factors, and Fourier transformation of an atomic ESP function results in an electron scattering length. An atomic ESP function is a sum of two ESP functions generated by Dirac δ-function nuclear charges and distributed electrons. The ESP of nuclear charges follows a Coulombic expression $\psi(r) = q/(4\pi\varepsilon_o r)$ in which the charge is in electron units and the distance in angstroms or the charge is in coulombs and the distance in meters (i.e., volts), and the negative charge of the distributed electrons is replaced by an integral of the electron probability density function in the same expression, where q is the charge, r is the distance to the nucleus, and ε_o is the dielectric constant in vacuum. When $r = 0$, the ESP for each of the nuclear and electron terms becomes infinite, but their sum for any neutral atom remains well-defined. As a result, the corresponding electron scattering length for any neutral atom is also well-determined at zero scattering angle even though they are not for any ionized atom. Cations have a positive infinite electron scattering length, and anions have a negative infinite length.

The Mn ions in the OEC of PSII are expected to have an ESP value much higher than that of protein atoms because the electron scattering length of a neutral Mn scatterer (7.506 Å at zero scattering angle) is at least 3 times that of common protein atoms (C, 2.509 Å; N, 2.211 Å; and O, 1.983 Å; see *International Tables for Crystallography*).[7] The disparity further increases when high oxidation states of Mn centers in the OEC are considered because ionic scattering lengths are determined at small scattering angles of $\sin \theta/\lambda < 0.05$ by the Coulombic charge term. Considering coordinate errors in an X-ray (and EM) structure determination, as well as errors due to X-ray-induced reduction of the OEC, it would be difficult to reliably assign atomic charges to the OEC for a computer simulation of the ESP function so that one may calculate an ESP function using only atomic scattering factors based on empirically assigned partial charges. In this study, we overcome that challenge by computing the ESP function with density functional theory (DFT), using DFT-optimized coordinates of the OEC in the dark-adapted S_1 state.[8] The resulting ESP is compared to experimental ESP maps recently reported using cryo-electron microscopy (EM),[5,6] to provide insights into changes in the ESP and thus in the occupancy of the OEC induced during electron irradiation in cryo-EM measurements. The ESP function was calculated on an optimized 353-atom cluster model of the OEC and its surrounding environment. The cluster model was based upon a two-layer quantum mechanics/molecular mechanics model of PSII in the S_1 state.[9] In total, 23 residues and 19 water molecules were included in the model along with the chloride anion bound to D2-K317. Residues included those directly bound to the OEC (D1-D170, -E189, -H332, -E333, -H337, -D342, and -A344 and CP43-E354 and -R357) along with several secondary shell residues (D1-D61, -N87, -Y_Z, -Q165, -S167, -S169, -G171,

-F182, -V185, -F186, -H190, and -N298 and D2-K317). The calculations were performed using DFT/B3LYP in the Gaussian 2009 software package.[10,11] To efficiently and accurately compute all atom types present, multiple basis sets were used. C, N, and H atoms were treated with 6-31G, O atom with 6-31G(d), Cl anion with 6-31+G(d), and metal ions (Mn and Ca) with the LanL2DZ pseudopotential and basis set.[12−16] The calculated ESP functions were examined and Gaussian-filtered using the graphics programs Chimera and Coot;[17,18] map manipulations were performed using the program CCP4 package,[19] and figures were made using PyMol.[20]

The experimental ESP maps (EMD 6617 and PDB 3JCU; EMD 6742 and PDB 5XNM), recently reported for PSII−LHCII supercomplexes at ~3.2 Å resolution, unexpectedly show that the ESP values at the OEC core are much lower than at the surrounding proteinaceous side chains (Figure 1).[5,6]
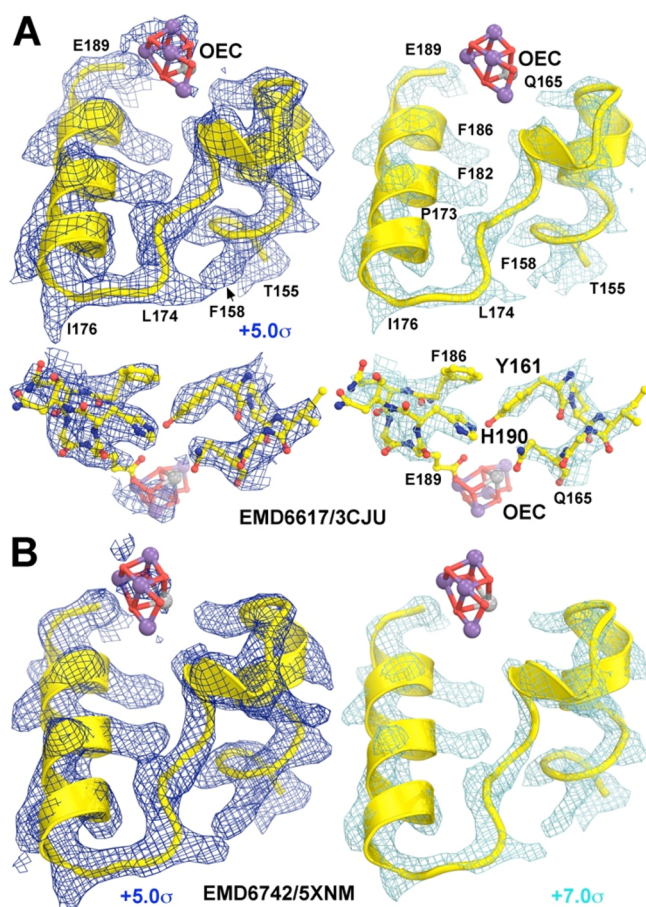

Figure 1. Experimental ESP maps obtained for the OEC of spinach PSII−LHCII supercomplexes contoured at 5.0σ (blue, left) and 7.0σ (cyan, right), superimposed on the corresponding atomic models. (A) EMD 6617 and PDB 3JCU.[5] (B) EMD 6742 and PDB 5XNM.[6]

When contoured at 7.0σ, the protein side chains are clearly visible continuously inside the iso-potential envelope whereas the OEC has no visible features. These differences are larger for the EMD 6742 model than for the EMD 6617 map, as quantified by the ESP ratio between the ESP of the OEC and the nearby reference side chain of amino acid residue D1-H190.

The asymptotic ESP ratio of neutral Mn and C scatterers can be obtained from the ratio of the zero-angle scattering lengths, as the corresponding ratio of the asymptotic electron density (ED) is obtained at zero scattering angle from the ratio of the total number of electrons.[21] However, for charged scatterers, the ESP ratio is also highly dependent on the net charge of the ions, especially at a small scattering angle,[22] which makes the ESP ratios difficult to predict when the partial charges of the scatterers are not accurately determined. Unfortunately, that is the case for the OEC of PSII because of the uncertainty in the precise coordinates of the ions and significant charge transfer interactions between the Mn ions and the oxo bridges. Here, we bypass those technical challenges by using DFT to obtain the ESP function of the OEC cluster after geometry optimization.

Another difficulty in the interpretation of experimental ESP maps is that the low-frequency structure factors are associated with a non-zero mean ESP value for water molecules in a "vitreous ice"-like state.[21] That difficulty can be overcome using charge density (CD) maps because the charge neutrality of any biomolecule ensures that the zero-frequency term will be zero for CD maps (even though not for ESP maps).[21,23,24]

The experimental EMD 6617 map[5] deposited in the EMD database has already been sharpened using a negative ΔB value (-150 Å^2), which alters the ESP ratio. However, this sharpening can be and was reversed. The negated Laplacian operation on the unsharpened ESP map results in an unmodified CD map.[21] The resulting CD map exhibits spatial resolution that is better than that of the sharpened ESP maps (Figure 2), as documented elsewhere.[24] In the case of the
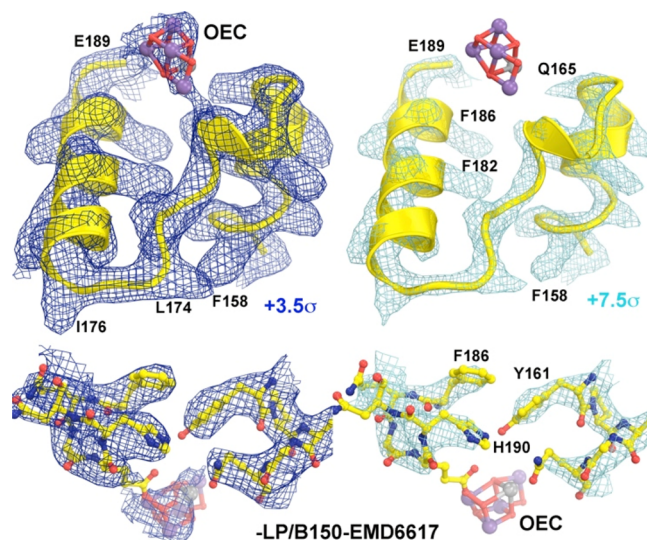

Figure 2. Experimental CD maps obtained for the OEC of spinach PSII−LHCII supercomplexes, contoured at 3.5σ (blue, left) and 7.5σ (cyan, right), superimposed on the atomic model (EMD 6617 and PDB 3JCU). The map has been unsharpened by $\Delta B = 150$ Å^2.

entire protein complex, with approximate charge neutrality, the mean CD value can be accurately determined. Thus, the corresponding relative occupancies of the subunits can be determined.[21]

For the OEC, charge neutrality may not be necessarily maintained so that the estimated CD and ESP ratios are only approximate. For that reason, it is important to use an internal reference (the nearby D1-H190 side chain) that allows for comparisons of CD and ESP peak ratios. Table 1 shows the comparison of ratios for both the original experimental EM

Table 1. Experimental ESP and CD Ratios between the OEC and the Side Chain of D1-H190 as a Function of Resolution in the Range of 3.2−5.0 Å[a]

	EMD 6617 and PDB 3JCU		EMD 6742 and PDB 5XNM	
Resolution	ESP	CD/B150	ESP	CD/B150
ESP0	0.55		0.44	
3.2 Å	0.65	0.56	0.54	0.54
3.6 Å	0.63	0.56	0.48	0.47
4.0 Å	0.57	0.53	0.55	0.43
4.5 Å	0.76	0.78	0.73	0.67
5.0 Å	0.78	0.72	0.64	0.54

[a]At a resolution lower than 4.0 Å, the effect of the net charge in the OEC becomes the determinant factor for the observed peak ratio but not necessarily for the occupancy. ESP0 represents the original ESP map, which was recalculated with the highest resolution indicated in the first column. The charge density map has been unsharpened using $\Delta B = 150$ Å^2.

maps and the recalculated EM maps at various resolution cutoffs. It shows that the CD ratio between the OEC and the side chain of residue D1-H190 does not change significantly from 3.2 to 4.0 Å resolution, maintaining a mean value of 0.55 ± 0.02 for the EMD 6617 map and 0.45 ± 0.02 for the EMD 6742 model. The ESP ratios prior to zero-frequency correction are 0.63 ± 0.04 and 0.52 ± 0.04 for the EMD 6617 and EMD 6742 maps, respectively, at the same resolution. The higher estimates of the ESP peak ratios, when compared to the CD peak ratios, are likely due to extra positive charges of the OEC ions relative to D1-H190 and the missing zero-frequency term, as discussed elsewhere.[21]

From ratios calculated at different resolutions, we decouple the contribution of varying occupancies from that of varying atomic B factors. The observation that the CD ratio does not change significantly over the analyzed resolution range suggests that the reduced CD ratio is not due to increased atomic B factors of the OEC atoms but rather primarily attributable to a reduced occupancy of the OEC.

To quantify the occupancy of the OEC, as influenced by reduction caused by electron irradiation during the cryo-EM measurements, we calculated the DFT ESP function of the OEC in the dark-adapted S_1 state (Figure 3A). The resulting ESP function was further subjected to Gaussian broadening with standard deviations of 0.50, 0.75, and 1.00 Å (Figure 3B–D, respectively, and Figure S1), corresponding to mean atomic B factors of 20, 44, and 79 Å^2 and effective resolutions of 1.7, 2.7, and 3.6 Å, respectively, according to an empirical relationship derived from protein X-ray structures.[24] The theoretical CD and ESP peak ratios between the OEC and the side chain of amino acid residue D1-H190 were evaluated (Table 2). Even at 3.6 Å resolution, the theoretical CD peak ratio is approximately 1.45, while at 1.7 Å resolution, it is 2.7. According to these theoretical values, the occupancy of the OEC is estimated to be 38% in the EMD 6617 map and 31% in the EMD 6742 map.[5,6]

Figure 3 shows that the appearance of the ESP map changes significantly with Gaussian broadening, B factor, and contouring level. For example, ordered water molecules are visible at a contour level of 4.0σ, when the atomic B factor is <20 Å^2 but not when B is >44 Å^2. Similarly, the chloride anion is visible when the B factor is <44 Å^2 but not when it is >79 Å^2 (Figure 3, Figure S1, and Table 2). For the minimum energy
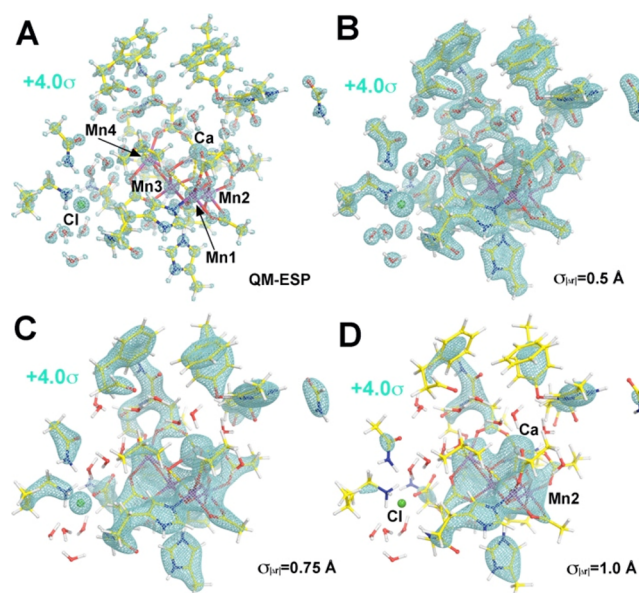

Figure 3. Theoretical ESP maps obtained (A) using DFT, convoluted with a Gaussian broadening function with root-mean-square displacements of (B) 0.5, (C) 0.75, and (D) 1.0 Å, contoured at 4.0σ, and superimposed on the atomistic model.

Table 2. Theoretical ESP and CD Ratios between the OEC and the Side Chain of Amino Acid Residue D1-H190 as a Function of the B Factor, Resolution, and Coordinate Displacement Used in Gaussian Filtering $\left[B = 8\pi^2(\sigma_{|\Delta r|})^2\right]$

	$\sigma_{|\Delta r|}$ (Å)	B value (Å^2)	resolution (Å)	ESP ratio	CD ratio
I	0.50	20	1.68	2.1	2.70
II	0.75	44	2.59	1.5	2.36
III	1.00	79	3.58	1.3	1.45

configuration of the OEC in the S_1 state, the nuclear coordinates are well-defined so one can examine the ESP function as a function of B value, either on an absolute scale or relative to an internal reference such as the Mn2 center (Figure S2), whose oxidation state remains constant during the catalytic cycle. On a relative scale, the ESP ratios provide some insight into the magnitudes of the charge differences between the atom of interest and the reference Mn2 center. For example, the chloride anion has a −1.0e charge, and its ESP ratio relative to that of the Mn2 center decreases rapidly as a function of increasing B factor; Ca^{2+} has a +2.0e charge (but a value smaller than that of the Mn2 center), and its ratio also decreases but with a reduced slope. The ESP ratios for all three of the other Mn centers relative to the internal Mn2 center are more complicated because of charge transfer interactions with the oxo bridges with negative partial atomic charges.

There was no apparent loss of the OEC during purification of samples from spinach leaves, which included a sucrose density gradient.[5] An oxygen evolution assay showed that band 9, which was used for cryo-EM studies, exhibited the same activity as those purified from *Arabidopsis*.[5] It is rather unexpected that the occupancies of two extrinsic subunits PsbQ and PsbP were found to be only ∼20% in the experimental ESP and CD maps derived from EMD 6714 for the PSII−LHCII supercomplex.[21] These two subunits play an important role in maintaining the integrity of the OEC, but

the step(s) in which they were lost remains unclear.[5,6] Therefore, the reduced occupancy of the OEC observed here in the cryo-EM structures of PSII−LHCII supercomplexes could result from either (i) particle-selection procedures during image reconstruction or (ii) electron-induced radiation damage during data acquisition. When the raw cryo-EM images were available like those for the *Thermoplasma acidophilum* proteasome, the $T_2 - T_1$ difference (i.e., late frames minus early frames in each particle image) Fourier method could be used to reveal electron radiation-induced changes in ESP functions,[25] which is beyond the scope of this study.

The reduced occupancy of the OEC observed here is likely to have happened during data acquisition because the ESP maps of other redox enzymes obtained by cryo-EM or electron crystallography show evidence of reduced redox centers. For example, the ESP of the heme iron bound in human hemoglobin exhibits a value much lower than the ESP of the surrounding protein environment as determined from the cryo-EM structure (Figure 4).[26] Similarly, it was also found that the
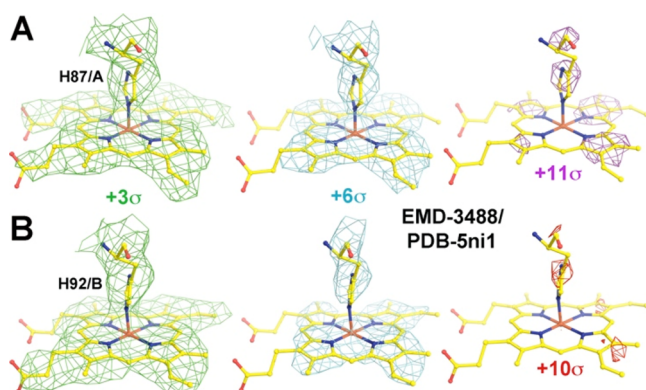

Figure 4. Experimental ESP maps measured for human hemoglobin, contoured at 3σ (green), 6σ (cyan), 11σ (magenta), and 10σ (red) for subunits A and B.[26]

ESP of the heme iron bound in catalase determined by using electron crystallography (PDB 3J7B, also at ∼3.2 Å resolution)[27] is much lower than for the nearby protein residues (Figure S3). In both examples, the affinity of Fe(III) for apo-heme is extremely high and so is the affinity of the heme for these proteins. It is extremely difficult to purify these proteins without heme or without Fe(III). Therefore, the loss of the ESP value at the Fe center must be associated with electron irradiation, which is likely to be controlled by redox potentials.

Given the fact that cryo-EM uses a dose much larger than that used during electron crystallography, it is likely that the OEC is reduced, leading to disorder and dissociation of metal centers during the electron scattering experiments. X-ray-induced reduction of the OEC has well been established in crystal structures of PSII during data acquisition at the liquid nitrogen temperature.[4] Byproducts of radiation-induced damage to protein samples caused by exposure to either X-rays or electron beams may bear some resemblance. Both might split water molecules into hydroxyl and hydrogenous free radicals, which are amplified by biological molecules or/ and other small organic molecules present in the samples. Both hydroxyl and hydrogen free radicals are very reactive, often resulting in redox-related modifications of proteins and redox

centers.[28,29] Furthermore, highly reducing hydrated electrons are specifically generated by inelastic scattering during electron irradiation of protein samples and cause dehydrogenation-like reactions, resulting in the release of large amounts of H_2.[30] Although there are some striking similarities in the consequences of electron and X-ray radiation-induced damage to protein samples as discovered in this study, the underlying chemistry likely differs, with one involving highly reductive, mobile hydrated electrons and the other involving both highly reactive, mobile hydrogenous and hydroxyl free radicals.[25]

■ ASSOCIATED CONTENT

Ⓢ Supporting Information

The Supporting Information is available free of charge on the ACS Publications website at DOI: 10.1021/acs.biochem.8b00609.

Three additional figures (PDF)

■ AUTHOR INFORMATION

Corresponding Author
*E-mail: jimin.wang@yale.edu.

ORCID Ⓘ
Jimin Wang: 0000-0002-4504-8038
Gary W. Brudvig: 0000-0002-7040-1892
Victor S. Batista: 0000-0002-3262-1237

Notes
The authors declare no competing financial interest.

■ ACKNOWLEDGMENTS

■ ABBREVIATIONS

CD, charge density; DFT, density functional theory; ED, electron density; EM, electron microscopy; ESP, electrostatic potential; LHC, light-harvesting complex; OEC, oxygen-evolving complex; PSII, photosystem II.

■ REFERENCES

(1) Umena, Y., Kawakami, K., Shen, J. R., and Kamiya, N. (2011) Crystal Structure of Oxygen-Evolving Photosystem II at a Resolution of 1.9 A. *Nature* 473, 55−60.

(2) Askerka, M., Brudvig, G. W., and Batista, V. S. (2017) The O2-Evolving Complex of Photosystem II: Recent Insights from Quantum Mechanics/Molecular Mechanics (QM/MM), Extended X-ray Absorption Fine Structure (EXAFS), and Femtosecond X-ray Crystallography Data. *Acc. Chem. Res.* 50, 41−48.

(3) Vinyard, D. J., and Brudvig, G. W. (2017) Progress Toward a Molecular Mechanism of Water Oxidation in Photosystem II. *Annu. Rev. Phys. Chem.* 68, 101−116.

(4) Yano, J., Kern, J., Irrgang, K. D., Latimer, M. J., Bergmann, U., Glatzel, P., Pushkar, Y., Biesiadka, J., Loll, B., Sauer, K., Messinger, J., Zouni, A., and Yachandra, V. K. (2005) X-ray Damage to the Mn4Ca Complex in Single Crystals of Photosystem II: a Case Study for

Metalloprotein Crystallography. *Proc. Natl. Acad. Sci. U. S. A. 102*, 12047−12052.

(5) Wei, X., Su, X., Cao, P., Liu, X., Chang, W., Li, M., Zhang, X., and Liu, Z. (2016) Structure of Spinach Photosystem II-LHCII Supercomplex at 3.2 A Resolution. *Nature 534*, 69−74.

(6) Su, X., Ma, J., Wei, X., Cao, P., Zhu, D., Chang, W., Liu, Z., Zhang, X., and Li, M. (2017) Structure and Assembly Mechanism of Plant C$_2$S$_2$M$_2$-type PSII-LHCII Supercomplex. *Science 357*, 815−820.

(7) Prince, E. (2004) *International Tables for Crystallography*, Vol. C, Kluwer Academic Publishers, London.

(8) Luber, S., Rivalta, I., Umena, Y., Kawakami, K., Shen, J. R., Kamiya, N., Brudvig, G. W., and Batista, V. S. (2011) S$_1$-state Model of the O2-Evolving Complex of Photosystem II. *Biochemistry 50*, 6308−6311.

(9) Askerka, M., Wang, J., Brudvig, G. W., and Batista, V. S. (2014) Structural Changes in the Oxygen-Evolving Complex of Photosystem II Induced by the S$_1$ to S$_2$ Transition: A Combined XRD and QM/MM study. *Biochemistry 53*, 6860−6862.

(10) Becke, A. D. (1993) Density-Functional Thermochemistry. III. The Role of Exact Exchange. *J. Chem. Phys. 98*, 5648−5652.

(11) Frisch, M. J., Trucks, G. W., Schlegel, H. B., Scuseria, G. E., Robb, M. A., Cheeseman, J. R., Scalmani, G., Barone, V., Petersson, G. A., Nakatsuji, H., Li, X., Caricato, M., Marenich, A., Bloino, J., Janesko, B. G., Gomperts, R., Mennucci, B., Hratchian, H. P., Ortiz, J. V., Izmaylov, A. F., Sonnenberg, J. L., Williams-Young, D., Ding, F., Lipparini, F., Egidi, F., Goings, J., Peng, B., Petrone, A., Henderson, T., Ranasinghe, D., Zakrzewski, V. G., Gao, J., Rega, N., Zheng, G., Liang, W., Hada, M., Ehara, M., Toyota, K., Fukuda, R., Hasegawa, J., Ishida, M., Nakajima, T., Honda, Y., Kitao, O., Nakai, H., Vreven, T., Throssell, K., Montgomery, J. A., Jr., Peralta, J. E., Ogliaro, F., Bearpark, M., Heyd, J. J., Brothers, E., Kudin, K. N., Staroverov, V. N., Keith, T., Kobayashi, R., Normand, J., Raghavachari, K., Rendell, A., Burant, J. C., Iyengar, S. S., Tomasi, J., Cossi, M., Millam, J. M., Klene, M., Adamo, C., Cammi, R., Ochterski, J. W., Martin, R. L., Morokuma, K., Farkas, O., Foresman, J. B., and Fox, D. J. (2016) *Gaussian 09*, Gaussian, Inc., Wallingford, CT.

(12) Ditchfield, R., Hehre, W. J., and Pople, J. A. (1971) Self-Consistent Molecular-Orbital Methods 0.9. Extended Gaussian-Type Basis for Molecular-Orbital Studies of Organic Molecules. *J. Chem. Phys. 54*, 724−728.

(13) Hehre, W. J., Ditchfield, R., and Pople, J. A. (1972) Self-Consistent Molecular-Orbital Methods 0.12. Further Extensions of Gaussian-Type Basis Sets for Use in Molecular-Orbital Studies of Organic-Molecules. *J. Chem. Phys. 56*, 2257−2261.

(14) Hariharan, Pc, and Pople, J. A. (1973) Influence of Polarization Functions on Molecular-Orbital Hydrogenation Energies. *Theor. Chim. Acta 28*, 213−222.

(15) Spitzngel, G. (1982) Ph.D. Thesis, Erlangen, Germany.

(16) Hay, P. J., and Wadt, W. R. (1985) Abinitio Effective Core Potentials for Molecular Calculations - Potentials for the Transition-Metal Atoms Sc to Hg. *J. Chem. Phys. 82*, 270−283.

(17) Yang, Z., Lasker, K., Schneidman-Duhovny, D., Webb, B., Huang, C. C., Pettersen, E. F., Goddard, T. D., Meng, E. C., Sali, A., and Ferrin, T. E. (2012) UCSF Chimera, MODELLER, and IMP: an Integrated Modeling System. *J. Struct. Biol. 179*, 269−278.

(18) Emsley, P., and Cowtan, K. (2004) Coot: Model-building Tools for Molecular Graphics. *Acta Crystallogr., Sect. D: Biol. Crystallogr. 60*, 2126−2132.

(19) Winn, M. D., Ballard, C. C., Cowtan, K. D., Dodson, E. J., Emsley, P., Evans, P. R., Keegan, R. M., Krissinel, E. B., Leslie, A. G., McCoy, A., McNicholas, S. J., Murshudov, G. N., Pannu, N. S., Potterton, E. A., Powell, H. R., Read, R. J., Vagin, A., and Wilson, K. S. (2011) Overview of the CCP4 suite and current developments. *Acta Crystallogr., Sect. D: Biol. Crystallogr. 67*, 235−242.

(20) DeLano, W. L. (2002) *The PyMOL Molecular Graphics System* (http://www.pymol.org/).

(21) Wang, J. (2018) Determination of Chemical Identity and Occupancy from Experimental Density Maps. *Protein Sci. 27*, 411−420.

(22) Wang, J., Liu, Z., Frank, J., and Moore, P. B. (2018) Identification of Ions in Experimental Electrostatic Potential Maps. *IUCrJ 5*, 375−381.

(23) Morse, P. M. (1932) The Non-Elastic Dispersion of Cathode Rays. *Phys. Z. 33*, 443−445.

(24) Wang, J. (2017) Experimental Charge Density from Electron Microscopic Maps. *Protein Sci. 26*, 1619−1626.

(25) Wang, J., Liu, Z., Crabtree, R. H., Frank, J., and Moore, P. B. (2018) On the Damage Done to the Structure of the *T. acidophiulm* Proteasome by Electron Radiation. *Protein Sci.*, DOI: 10.1002/pro.3511.

(26) Khoshouei, M., Radjainia, M., Baumeister, W., and Danev, R. (2017) Cryo-EM Structure of Haemoglobin at 3.2 angstrom Determined with the Volta Phase Plate. *Nat. Commun. 8* (1−6), 16099.

(27) Nannenga, B. L., Shi, D., Hattne, J., Reyes, F. E., and Gonen, T. (2014) Structure of Catalase Determined by MicroED. *eLife 3*, No. e03600.

(28) Wang, J. (2016) X-ray Radiation-Induced Addition of Oxygen Atoms to Protein Residues. *Protein Sci. 25*, 1407−1419.

(29) Wang, J. (2016) Oxygen Additions in Serial Femtosecond Crystallographic Protein Structures. *Protein Sci. 25*, 1797−1802.

(30) Leapman, R. D., and Sun, S. Q. (1995) Cryoelectron Energy-Loss Spectroscopy - Observations on Vitrified Hydrated Specimens and Radiation-Damage. *Ultramicroscopy 59*, 71−79.